

# Kinetics of apatite formation on a calcium-silicate cement for root-end filling during ageing in physiological-like phosphate solutions

Maria Giovanna Gandolfi · Paola Taddei · Anna Tinti ·  
Elettra De Stefano Dorigo · Piermaria Luigi Rossi ·  
Carlo Prati

Received: 27 January 2009 / Accepted: 10 November 2009 / Published online: 27 November 2009  
© Springer-Verlag 2009

**Abstract** The bioactivity of calcium silicate mineral trioxide aggregate (MTA) cements has been attributed to their ability to produce apatite in presence of phosphate-containing fluids. This study evaluated surface morphology and chemical transformations of an experimental accelerated calcium-silicate cement as a function of soaking time in different phosphate-containing solutions. Cement discs were immersed in Dulbecco's phosphate-buffered saline (DPBS) or Hank's balanced salt solution (HBSS) for different times (1–180 days) and analysed by scanning electron microscopy connected with an energy dispersive X-ray analysis (SEM-EDX) and micro-Raman spectroscopy. SEM-EDX revealed Ca and P peaks after 14 days in DPBS. A thin Ca- and P-rich crystalline coating layer was detected after 60 days. A thicker multilayered coating was observed after 180 days. Micro-Raman disclosed the 965-cm<sup>-1</sup> phosphate band at 7 days

only on samples stored in DPBS and later the 590- and 435-cm<sup>-1</sup> phosphate bands. After 60–180 days, a layer ~200–900 μm thick formed displaying the bands of carbonated apatite (at 1,077, 965, 590, 435 cm<sup>-1</sup>) and calcite (at 1,088, 713, 280 cm<sup>-1</sup>). On HBSS-soaked, only calcite bands were observed until 90 days, and just after 180 days, a thin apatite–calcite layer appeared. Micro-Raman and SEM-EDX demonstrated the mineralization induction capacity of calcium-silicate cements (MTAs and Portland cements) with the formation of apatite after 7 days in DPBS. Longer time is necessary to observe bioactivity when cements are immersed in HBSS.

**Keywords** Calcium-silicate cements · MTA cements · Portland cement · Ageing · Phosphate solutions · Apatite · Calcite

M. G. Gandolfi · C. Prati  
Laboratory of Biomaterials and Oral Pathology,  
Department of Odontostomatological Science,  
Endodontic Clinical Section, University of Bologna,  
Bologna, Italy

M. G. Gandolfi (✉) · P. L. Rossi  
Department of Earth Sciences, University of Bologna,  
Bologna, Italy  
e-mail: mgiovanna.gandolfi@unibo.it

P. Taddei · A. Tinti  
Department of Biochemistry, University of Bologna,  
Bologna, Italy

E. De Stefano Dorigo  
Unit of Dental Sciences and Biomaterials, Department of  
Biomedicine, University of Trieste,  
Trieste, Italy

## Introduction

Calcium-silicate cements, such as mineral trioxide aggregate (MTA) and others [1], demonstrated a wide range of clinical applications including root-end filling material, root perforation repair, pulp capping and dentine hypersensitivity [2–6]. As stated by the patent, MTA is a derivative of a type I ordinary Portland cement with 4:1 proportions of bismuth oxide added for radiopacity. Portland cement is the active ingredient in white MTA [7]. White Portland cements are hydraulic materials mainly composed of di- and tricalcium silicate (2CaO·SiO<sub>2</sub> belite and 3CaO·SiO<sub>2</sub> alite), tricalcium aluminate 3CaO·Al<sub>2</sub>O<sub>3</sub> and gypsum CaSO<sub>4</sub>·2 H<sub>2</sub>O hydrophilic powders. When hydrated, the silicate phases of Portland cements (and MTA) undergo a series of physicochemical reactions resulting in the forma-

tion of a nanoporous matrix/gel of calcium silicate hydrates (“C–S–H phases”) and of a soluble fraction of calcium hydroxide  $\text{Ca}(\text{OH})_2$  or portlandite [1, 8].

The bioactivity of Portland cement in phosphate buffered solutions has been recently reported [9–12]. Recent investigations have reported that Portland cements release calcium and when immersed in phosphate solutions induce apatite formation and produce high alkalinity in the surrounding environment [9–12]. Moreover, Portland cements may remineralize the partially demineralized dentine and induce calcium-phosphate deposits formation [13].

Besides these advantages, Portland cements and MTA also have some drawbacks, when used as endodontic material. The major problem lies in their extended setting time [14–16] and difficult handling. Reduction in setting time could be advantageous in endodontics, as allows an earlier dental reconstruction. Therefore, the composition of Portland cements should be adjusted and properly modified to avoid these drawbacks. Calcium chloride accelerates the reaction between tricalcium aluminate and gypsum, and it has been demonstrated that the addition of calcium chloride reduce the setting time of Portland cements [17–19].

In the present study, a new accelerated cement based on white Portland cement has been prepared. Both scanning electron microscopy connected with energy dispersive X-ray analysis (SEM-EDX) and micro-Raman analyses were used to investigate the surface morphology and composition of the cement after ageing for different times in two physiological-like phosphate solutions.

To our knowledge, no previous research has assessed the apatite-like formation directly on the cement surface and analysed the bioactivity of modified Portland cements. Furthermore, this is the first study regarding the kinetics of formation–transformation of biocoating on Portland cement over time (from few hours to 180 days). The originality of this investigation is: (1) the long-term study on the bioactive behaviour of Portland cement, (2) the use of both high and low phosphate-containing soaking solutions, (3) the chemical and morphological typification of the outer surfaces over time and (4) the use of micro-Raman technique.

## Materials and methods

### Cement samples

An experimental thermally and mechanically treated calcium-silicate cement (identified as wTC) composed of white Portland cement (CEM I, Aalborg, Denmark) and calcium chloride 5% *w/w* was prepared. The white Portland cement contains the main active ingredients (tricalcium

silicate and dicalcium silicate) of MTAs (white ProRoot MTA and MTA-Angelus). Commercial MTAs were not used in this study for the interferences of bismuth oxide (added as radio-opacifier agent) with micro-Raman analysis (in particular with the detection of the portlandite band).

The cement was mixed with water and layered on a plastic cover-slip with 13 mm diameter (Thermanox Plastic, Nalge Nunc International, NY, USA) to obtain standard discs. Mechanical vibrations were used to obtain a flat regular surface. The exposed surface area of the discs was  $1.9 \pm 0.1 \text{ cm}^2$  with a thickness of approx. 0.9 mm. Immediately after preparation, the samples were placed in physiological-like storage solutions at 37°C, Dulbecco’s phosphate-buffered saline (DPBS) and Hank’s balanced salt solution (HBSS).

DPBS (Cambrex Bio Science Verviers s.p.r.l., Belgium, cat. n.BE17-512) is a physiological-like buffered (pH 7.4) Ca- and Mg-free solution with the following composition (mM):  $\text{K}^+$  (4.18),  $\text{Na}^+$  (152.9),  $\text{Cl}^-$  (139.5),  $\text{PO}_4^{3-}$  (9.56) (sum of  $\text{H}_2\text{PO}_4^-$  1.5 mM and  $\text{HPO}_4^{2-}$  8.06 mM).

HBSS solution (pH 7.4, Cambrex Bio Science Verviers s.p.r.l., Belgium, cat. n.10-527) reported the following composition (mM):  $\text{Ca}^{2+}$  (1.27),  $\text{Cl}^-$  (144.7),  $\text{K}^+$  (5.8)  $\text{Na}^+$  (141.6),  $\text{Mg}^{2+}$  (0.81),  $\text{HCO}_3^-$  (4.17),  $\text{SO}_4^{2-}$  (0.81),  $\text{PO}_4^{3-}$  (0.776) (sum of  $\text{H}_2\text{PO}_4^-$  0.44 mM and  $\text{HPO}_4^{2-}$  0.336 mM).

DPBS is a calcium-free and phosphate-rich (9.56 mM) solution where the release of calcium ions from the cements was the limiting parameter in the precipitation reaction [12], and the high amount of phosphate represents the continuous replenishment of phosphate ions from tissue fluids. Differently, HBSS contains calcium and lower phosphate. Commercial media were selected because they are standardised and readily available.

The endpoint times were 1, 3, 7, 14, 21, 28, 60, 90 and 180 days. The soaking media were renewed weekly.

### SEM-EDX

All samples were removed from the solution and dried at 37°C for 12 h. Specimens were then coated with carbon before being examined by a scanning electron microscope equipped with EDX (SEM-EDX 515, Phillips, Eindhoven, The Netherlands) using an accelerating voltage of 5–20 keV. The electron beam penetration at 20-keV acceleration was 2.98  $\mu\text{m}$ , and the volume excited with a density of 3  $\text{g}/\text{cm}^3$  must be considered 2.30  $\mu\text{m}^3$ . The *x*-axis of the EDX spectra displays the energy of the X-ray in KeV; the *y*-axis displays the intensity of the X-ray signal (counts).

### Micro-Raman spectroscopy

Micro-Raman spectra were obtained using a Jasco NRS-2000C instrument connected to a microscope with  $\times 20$

magnification (in these conditions the laser spot size was about 5  $\mu\text{m}$ ). All the spectra were recorded in back-scattering conditions with 5  $\text{cm}^{-1}$  spectral resolutions using the 488 nm line (Innova Coherent 70) with a power of 50 mW. A 160 K frozen CCD detector from Princeton Instruments, Inc. was used. The laser penetration in cement was about 10  $\mu\text{m}$ . To minimise the variability deriving from possible sample inhomogeneity, five spectra at least were recorded on five different points of each specimen area (i.e. upper surface, inner fractured side). In addition, the powder dispersed in the medium at selected storage times was isolated and at least five spectra were recorded. Raman spectra were also recorded on unhydrated powder of cements. The cements were analysed as wet samples when maintained in their storage media.

#### pH measurements

The pH of the soaking solutions was measured with a Denver Instrument Basic pH metre equipped with a Hamilton liq-glass electrode and  $\pm 0.01$  resolution. The electrode was inserted into the soaking solutions at room temperature (24°C). Each measurement was repeated three times. The mean pH was then plotted against time.

## Results

### SEM

SEM-EDX analysis showed different surface morphologies depending on the soaking solution and ageing time. The Ca/Si and Ca/P ratios calculated from the spectra have not been judged reliable, since unfortunately, the EDX spectra never reflected the composition of a unique phase. Calcite can be considered present in all the spectra, and it is hard to eliminate its contribution. At the same time, the high X-ray penetration under thin deposits made detectable the Si peak assignable to the underneath cement matrix.

Samples aged in DPBS for 1 day showed an amorphous irregular outer surface free from visible deposits. EDX detected high calcium (Ca) and somewhere silicon (Si) peaks. Samples aged for 3–7 days presented many prismatic/cubic crystals on the surface. EDX revealed Ca peaks. Diffuse larger hexagonal and cubic crystals were detected on the cement surface after 14 days of DPBS immersion (Fig. 1a). Many thin bright cloud-like deposits were detected on the cement surface. EDX of the area revealed Ca and low P reflexes. Punctual microanalyses detected high Ca and P peaks on cloud-like deposits and only Ca peaks on prismatic crystals (Fig. 1a). A thick

continuous granular layer showing a porous finely granular structure was detected after 28–60 days of DPBS immersion. EDX revealed Ca and P peaks on the entire surface. After 90–180 days, the surface deposit appeared thicker (Fig. 2a) and adherent to the cement surface as a thick coating layer. EDX revealed Ca and P peaks. Silicon reflexes were no longer detectable after 21 days of immersion.

Cements soaked in HBSS for 1 day showed an amorphous outer surface. EDX revealed Ca peaks and rare traces of Si. At 3–7 days of immersion, the surface became more homogeneous with small crystals. EDX revealed high Ca peak. Rounded-globular and prismatic-cubic Ca-rich crystals varying in size were observed on samples stored for 14–28 days (Fig. 1b). After 60–90 days cloud-like deposits were occasionally detected on a prismatic-cubic crystal layer (Fig. 2b). The deposits, not uniformly distributed, were composed of light P-containing precipitates and cube-like and/or polygonal Ca-rich crystals. EDX of the area revealed Ca peaks. Punctual EDX analysis of cloud-like deposits revealed Ca and P peaks (Fig. 2b). After 180 days, the surface was covered by a porous inhomogeneous Ca- and P-rich coating layer formed by a light porous matrix with interspersed polygonal crystals partially inserted into the coating.

A dense homogeneous structure with rare porosities was observed in the inner area in all the fractured samples aged for 1–180 days in both solutions. Needle-like crystals were occasionally disclosed. EDX of the internal area revealed Ca, Si and traces of aluminium (Al) peaks (Fig. 3).

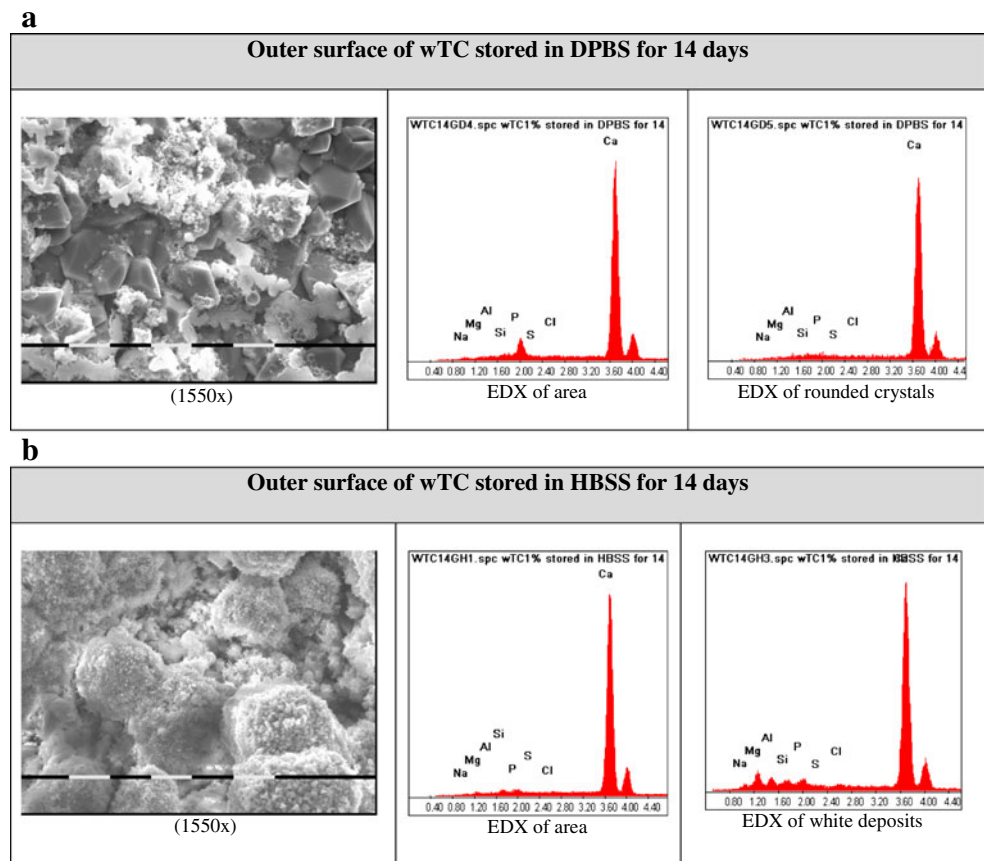
### Micro-Raman spectroscopy

Many chemical modifications were observed on the cement surface in relation to the soaking solution and the ageing time (Tables 1 and 2 and Figs. 4 and 5). Band assignments reported in the Tables and Fig. 4 have been made according to the literature [20–24].

No phosphate band (965  $\text{cm}^{-1}$ ,  $\nu_1 \text{PO}_4^{3-}$  stretching mode [20]) was detected in the unhydrated powder ( $t=0$ , Fig. 4a, spectrum a).

The micro-Raman spectra recorded on the surface of the samples stored for 1–3 days in DPBS (Fig. 3a, spectrum b) disclosed the bands of ettringite (991  $\text{cm}^{-1}$   $\nu_1 \text{SO}_4^{2-}$  stretching mode [21]), gypsum (1,004  $\text{cm}^{-1}$   $\nu_1 \text{SO}_4^{2-}$  stretching mode [22]), alite and belite (860–848  $\text{cm}^{-1}$   $\nu_1 \text{SiO}_4^{4-}$  [23]) and hydrated silicates (670  $\text{cm}^{-1}$ , Si–O–Si bending mode [23], very weak and only occasionally detected), carbonate ions in different chemical phases ( $\nu_1 \text{CO}_3^{2-}$  stretching bands at 1,088  $\text{cm}^{-1}$  for calcite and/or aragonite and at 1,075  $\text{cm}^{-1}$  for vaterite [25]) and the disappearance of the anhydrite bands at 1,019 and 677  $\text{cm}^{-1}$  ( $\nu_1 \text{SO}_4^{2-}$  stretching and  $\nu_4 \text{SO}_4^{2-}$  bending modes, respectively [22]). No bands of portlandite

**Fig. 1** SEM-EDX analysis of wTC surface after a soaking period of 14 days (*bar* 10  $\mu\text{m}$ ), showing apatite and calcite deposits in DPBS (**a**) and calcite coating layer in HBSS (**b**). The *x*-axis displays the energy of the X-ray in KeV, and the *y*-axis displays the intensity of the X-ray signal (counts)



( $360\text{ cm}^{-1}$ , due to Ca-O polyhedra vibrations) [25] or phosphate ( $965\text{ cm}^{-1}$ ) [20] were detected. The  $965\text{-cm}^{-1}$  phosphate band was detected in the powder isolated from the storage medium. After 7 days of storage in DPBS, this band occasionally appeared also on the surface of the cement (Fig. 4a, spectrum c), while after 14 days it was detected in all the recorded spectra indicating that the apatite deposit was present on the entire surface. After 7–14 days in DPBS, cement bands at  $991$  and  $860\text{ cm}^{-1}$  were still visible and crystalline calcite (bands at  $1,088$ ,  $713$ ,  $280\text{ cm}^{-1}$ , assignable to  $\nu_1$ ,  $\nu_4\text{ CO}_3^{2-}$  and lattice vibrations, respectively [25]) was present. No portlandite band ( $360\text{ cm}^{-1}$ ) was detected.

The samples stored in DPBS for longer times (after 28 days, Fig. 4a, spectrum e) also displayed the phosphate bands at  $590$  and  $435\text{ cm}^{-1}$  ( $\nu_2\text{ PO}_4^{3-}$  and  $\nu_4\text{ PO}_4^{3-}$  bending modes, respectively [20]). The band at  $1,077\text{ cm}^{-1}$  ( $\nu_1\text{ CO}_3^{2-}$  stretching) typical of carbonated apatite [20] was detected after 60 days (Fig. 4a, spectra f and g).

At 180 days, the cement bands were no longer visible due to the thicker surface deposit: only carbonated apatite and calcite were detected (Fig. 4a, spectrum g). Raman analysis showed that at increasing storage times in DPBS, the apatite deposit became progressively thicker, as revealed by the progressive increase in intensity of the

$965\text{ cm}^{-1}$  band with respect to the cement bands (Fig. 4a). The  $I_{965}/I_{990}$  phosphate/cement intensity ratio was calculated to evaluate the thickness of the deposit (Fig. 5): the rise in this ratio indicated the increase in the deposit thickness on the cement surface. The thickness of the apatite deposit was estimated by recording micro-Raman spectra every  $100\text{ }\mu\text{m}$  in the inner fractured side beginning at the surface. The thickness of the apatite deposit on cement was approx.  $200\text{ }\mu\text{m}$  after 60 days and approx.  $900\text{ }\mu\text{m}$  after 180 days.

Portlandite band ( $360\text{ cm}^{-1}$ ) was not found on the cement upper surface (Fig. 4) and was detected only in the inner fractured surface of the samples.

As regards ageing in HBSS, the bands of calcite deposit were observed from 1 to 180 days (Fig. 4b). The cement bands were no longer detectable on the sample surfaces after 60 days (Fig. 4b, spectra c and d). No phosphate band ( $965\text{ cm}^{-1}$ ) was detected on the upper surface until 180 days. However, the  $965\text{-cm}^{-1}$  phosphate band was detected in the powder isolated from the storage medium after 14 days. At 180 days, the phosphate band was also detected on the upper surface (Fig. 4b, spectrum d), indicating a sufficiently thick apatite deposit (less than  $50\text{ }\mu\text{m}$  thick). In addition, many crystalline calcite deposits were also noticed.

**Fig. 2** SEM-EDX analysis of wTC surface after a soaking period of 90 days (*bar* 10  $\mu\text{m}$ ), showing a thick apatite coating in DPBS (**a**), calcite and apatite/calcite coating in HBSS (Si reflex due to the underlying cement is visible because of the deep X-ray penetration under the deposit) (**b**). X-ray energy (KeV) on *x*-axis and X-ray signal (counts) on *y*-axis

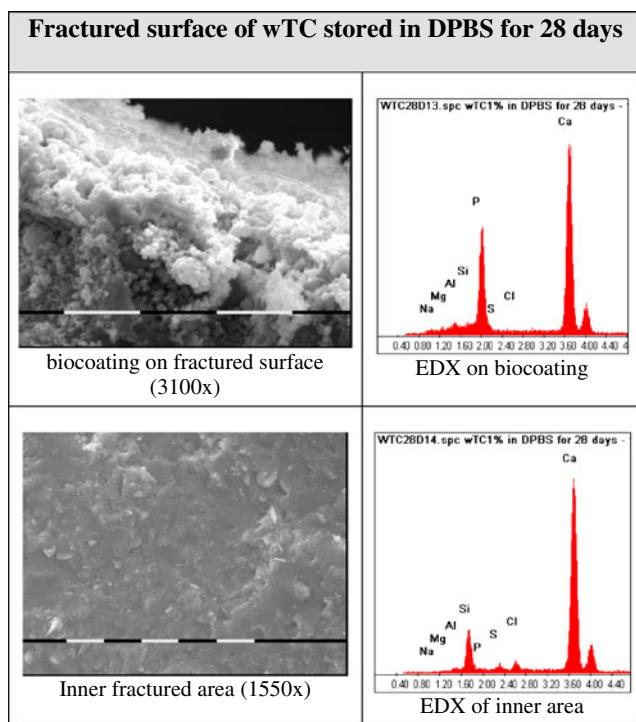
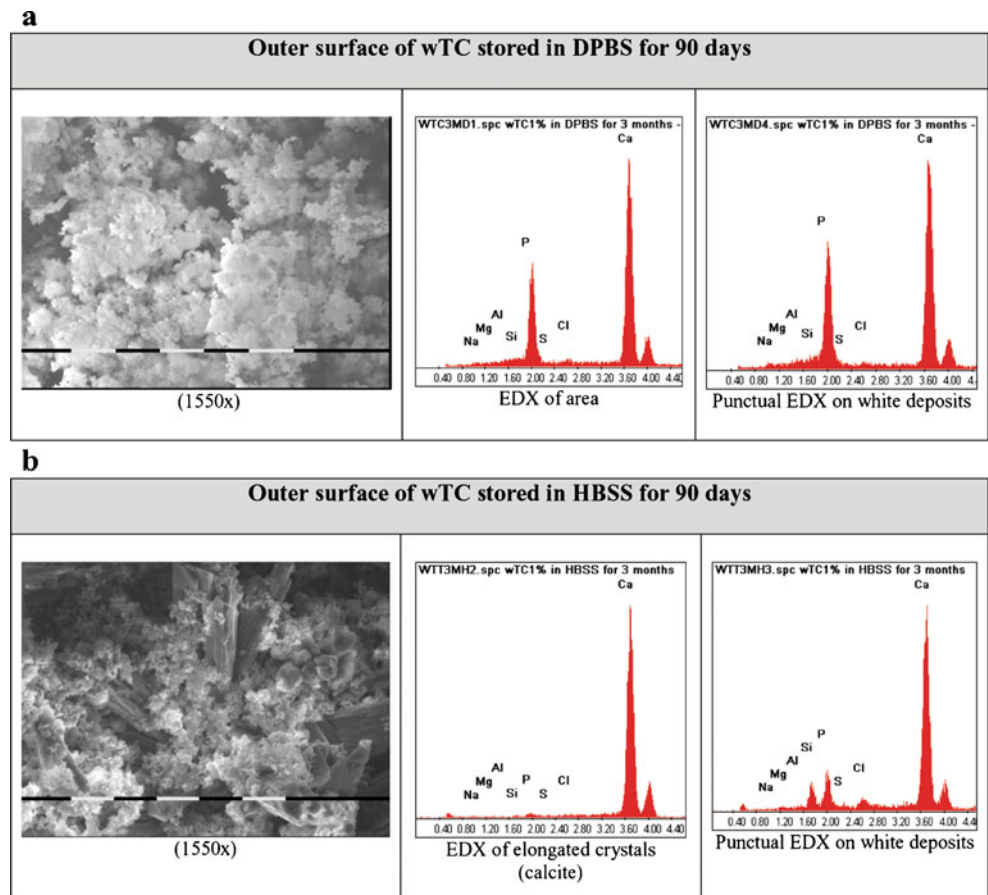


**Fig. 3** Fractured disc showing the thick biocoating on cement surface (*bar* 10  $\mu\text{m}$ )

**pH measurements**

Figure 6 shows the pH values of the two ageing media. At 24 h, the pH was very high (approx. 11.9) in both solutions. Thereafter, the pH was more than 12 until 7 days and slowly decreased to about 9 at 28 days. At 180 days, the pH was 9.0 in DPBS and 8.2 in HBSS.

**Discussion**

This study demonstrated that calcium-silicate cements aged in physiological-like phosphate solutions produce a superficial biocoating formed by carbonated apatite and calcite deposits.

A marked bioactivity of experimental cement was found in DPBS. DPBS solution has been previously used in Portland cement-DPBS systems [12, 26]. The high amount of phosphate represents the continuous replenishment of phosphate ions from tissue fluids [12, 26], and the absence of calcium makes the release of calcium ions from the cements the limiting parameter in the precipitation reaction [12]. Long immersion time (i.e. 180 days) in DPBS created the conditions for the formation of a thick carbonated apatite layer (approx. 900  $\mu\text{m}$  thick). Micro-Raman

**Table 1** Summary of the most significant information obtained by micro-Raman spectra recorded on the upper surface of the wTC cement during ageing in DPBS and HBSS (0–7 days)

Ageing time	DPBS	HBSS
<i>t</i> =0 unhydrated cement	Alite: bands at 848 cm <sup>-1</sup> ( $\nu_1$ SiO <sub>4</sub> <sup>4-</sup> ), 539–523 cm <sup>-1</sup> ( $\nu_4$ SiO <sub>4</sub> <sup>4-</sup> ) Belite: bands at 979 cm <sup>-1</sup> ( $\nu_3$ SiO <sub>4</sub> <sup>4-</sup> ), 856–848 cm <sup>-1</sup> ( $\nu_1$ SiO <sub>4</sub> <sup>4-</sup> ), 553–539–523 cm <sup>-1</sup> ( $\nu_4$ SiO <sub>4</sub> <sup>4-</sup> ) Gypsum: band at 1,004 cm <sup>-1</sup> ( $\nu_1$ SO <sub>4</sub> <sup>2-</sup> ) Anhydrite: bands at 1,019 cm <sup>-1</sup> ( $\nu_1$ SO <sub>4</sub> <sup>2-</sup> ), 677 cm <sup>-1</sup> ( $\nu_4$ SO <sub>4</sub> <sup>2-</sup> ) Calcium carbonate: band at 1,089 cm <sup>-1</sup> ( $\nu_1$ CO <sub>3</sub> <sup>2-</sup> )	
1 day	Disappearance of the bands of anhydrite (1,019, 677 cm <sup>-1</sup> ) Appearance of the band at 991 cm <sup>-1</sup> (ettringite, $\nu_1$ SiO <sub>4</sub> <sup>4-</sup> ): lower content than in the inner fractured side Decrease in intensity of the component at 848 cm <sup>-1</sup> (alite and belite) with respect to the 860 cm <sup>-1</sup> band (belite): alite hydrates more rapidly than belite Carbonate ions in different chemical environments: calcite and/or aragonite (1,088 cm <sup>-1</sup> ) and vaterite (1,075 cm <sup>-1</sup> ) No bands of portlandite (360 cm <sup>-1</sup> , Ca–O polyhedra vibrations) No phosphate band detected (965 cm <sup>-1</sup> , $\nu_1$ PO <sub>4</sub> <sup>3-</sup> ) Phosphate band at 965 cm <sup>-1</sup> detected in the powder isolated from the storage medium	Phosphate band at 965 cm <sup>-1</sup> not detected in the powder isolated from the storage medium
3 days	Cement: ettringite (991 cm <sup>-1</sup> ), gypsum (1,004 cm <sup>-1</sup> ), alite and belite (860–848 cm <sup>-1</sup> ), hydrated silicates (670 cm <sup>-1</sup> , Si–O–Si bending) Carbonate ions in different chemical environments: calcite and/or aragonite (1,088 cm <sup>-1</sup> ) and vaterite (1,075 cm <sup>-1</sup> ) No bands of portlandite (360 cm <sup>-1</sup> ) No phosphate band detected (965 cm <sup>-1</sup> ) Phosphate band at 965 cm <sup>-1</sup> detected in the powder isolated from the storage medium	Phosphate band at 965 cm <sup>-1</sup> not detected in the powder isolated from the storage medium
7 days	Disappearance of the 1,004 cm <sup>-1</sup> band (gypsum consumed) Bands of the cement still observable Increase in crystallinity of the calcium carbonate component: calcite (1,088, 713, 280 cm <sup>-1</sup> ) No bands of portlandite (360 cm <sup>-1</sup> ) Appearance of the 965 cm <sup>-1</sup> phosphate band (one of the five recorded spectra on the upper surface, poorly homogeneous apatite deposit)	No phosphate band detected (965 cm <sup>-1</sup> ) either on the upper surface or in the powder isolated from the storage medium

Band assignments have been given according to the literature [20–24]

spectroscopy identified the crystalline and amorphous phases of both the outer surface and inner bulk of the cement after hydration reaction whereas SEM-EDX revealed their morphology and elemental composition.

The potential of Raman spectroscopy to characterise cements has been used to investigate cement hydration *in situ* and in real-time with no sample manipulation and minimal interference from the water environment [25, 27]. Micro-Raman configuration monitors changes in chemical composition and morphology on a micro-scale since the laser spot (i.e. the excitation source) size is of the order of a few microns. SEM-EDX may be used to detect cement surface morphology [12] and to evaluate the chemical modifications induced by immersing cements in body fluid solutions for different times.

Although Raman spectroscopy has been widely applied to the study of the hydration mechanism of cements [24, 25, 27], this is the first study which uses

Raman technique to investigate the ageing of cements in phosphate-containing solutions. The findings obtained in the present study are in general agreement with the results reported in the literature as concerns the formed products [24, 25, 27]. As summarised in Table 1, after 1 day of ageing, the component at 848 cm<sup>-1</sup> (alite and belite) was found to decrease in intensity with respect to the 860 cm<sup>-1</sup> band (belite); this trend confirmed that alite hydrated more rapidly than belite, according to the literature [24, 25, 27].

The different behaviour of the sulphate bands due to gypsum and anhydrite (Table 1) indicated that the latter reacted more rapidly than the former and after 1 day of storage was completely consumed. An opposite result was found by Gastaldi et al. [24] for calcium sulphoaluminate cements aged in water. Our results indicated that ettringite formed at expenses of anhydrite and possibly, more slowly, of gypsum.

**Table 2** Summary of the most significant information obtained by micro-Raman spectra recorded on the upper surface of the wTC cement during ageing in DPBS and HBSS (14–180 days)

Ageing time	DPBS	HBSS
14 days	Bands of the cement still observable Calcite (1,088, 713, 280 $\text{cm}^{-1}$ , assignable to $\nu_1$ , $\nu_4$ $\text{CO}_3^{2-}$ and lattice vibrations, respectively) No bands of portlandite (360 $\text{cm}^{-1}$ ) 965 $\text{cm}^{-1}$ phosphate band observable in all the recorded spectra (homogeneous apatite deposit)	No phosphate band detected (965 $\text{cm}^{-1}$ ) on the upper surface (phosphate band detected in the powder isolated from the storage medium)
21-28 days	Bands of the cement still observable Calcite (1,088, 713, 280 $\text{cm}^{-1}$ ) No bands of portlandite (360 $\text{cm}^{-1}$ ) Apatite (bands at 965, 590 $\text{cm}^{-1}$ ( $\nu_2$ $\text{PO}_4^{3-}$ ), 435 $\text{cm}^{-1}$ ( $\nu_4$ $\text{PO}_4^{3-}$ )) + calcite deposit	Calcite deposit No phosphate band detected (965 $\text{cm}^{-1}$ ) on the upper surface (phosphate band detected in the powder isolated from the storage medium)
60 days	Calcite (1,088, 713, 280 $\text{cm}^{-1}$ ) No bands of portlandite (360 $\text{cm}^{-1}$ ) Carbonated (1,077 $\text{cm}^{-1}$ , $\nu_1$ $\text{CO}_3^{2-}$ , well visible) apatite (~200 $\mu\text{m}$ thick) + calcite deposit Bands of the cement still observable	Calcite deposit No phosphate band detected (965 $\text{cm}^{-1}$ ) on the upper surface (phosphate band detected in the powder isolated from the storage medium) Bands of the cement no longer detectable
90 days	Calcite (1,088, 713, 280 $\text{cm}^{-1}$ ) No bands of portlandite (360 $\text{cm}^{-1}$ ) Carbonated apatite (~300 $\mu\text{m}$ thick) + calcite deposit Bands of the cement still observable	Calcite deposit No phosphate band detected (965 $\text{cm}^{-1}$ ) on the upper surface (phosphate band detected in the powder isolated from the storage medium) Bands of the cement no longer detectable
180 days	Bands of the cement no longer observable (thicker deposit) No bands of portlandite (360 $\text{cm}^{-1}$ ) Carbonated apatite (~900 $\mu\text{m}$ thick) + calcite deposit	Apatite (965 $\text{cm}^{-1}$ phosphate band detected also on the upper surface, less than 50 $\mu\text{m}$ thick) + calcite deposit

Band assignments have been given according to the literature [20–24]

The hydration reaction of Portland cement produces calcium silicate (C–S–H) gel and a large amount of calcium hydroxide [1, 8, 28]. The latter component can be easily detected by Raman spectroscopy (if the cement is devoid of bismuth oxide), while the former is characterised by a weak Raman spectrum, due to the amorphous nature of C–S–H. During the hydration reaction, the soluble calcium hydroxide formed rapidly dissolves from the cement surface by continuous washout in solution [11, 12], as demonstrated by the absence of the portlandite Raman band (360  $\text{cm}^{-1}$ ) on the upper surface of the cement. Also, the pH increase of the storage medium confirmed that calcium hydroxide was washed away by the storage medium. At 24 h, the pH was very high in both solutions (about 11.9) in agreement with Tay et al. for PBS [12]. At 180 days, the pH was 9.0 in DPBS and 8.2 in HBSS indicating that the amount of portlandite released by the cement slowly decreased with time and that  $\text{Ca}(\text{OH})_2$  was released faster into the HBSS

solution. Moreover, the  $\text{OH}^-$  ions released are probably partially buffered by the solution.

However, the increase in pH and the high concentration of  $\text{Ca}^{2+}$  ions [11] enhance the supersaturation of the solution with respect to apatite and promote the precipitation of the carbonated apatite coating layer on the cement surface. Calcium release may be biologically important in several clinical applications such as pulp capping procedures and apicogenesis [6, 29, 30]. Calcium hydroxide is a well-known antibacterial agent of value in many clinical conditions such as in infected root canals when used as root canal dressing [31].

SEM-EDX of the samples immersed in DPBS for 3–14 days disclosed Ca peaks in prismatic-cubic crystals, likely calcite, as indicated by micro-Raman analysis. Interestingly, after 14 days, cloud-like granular Ca- and P-rich deposits appeared at SEM-EDX. The Raman band at 965  $\text{cm}^{-1}$  confirmed the formation of calcium phosphate

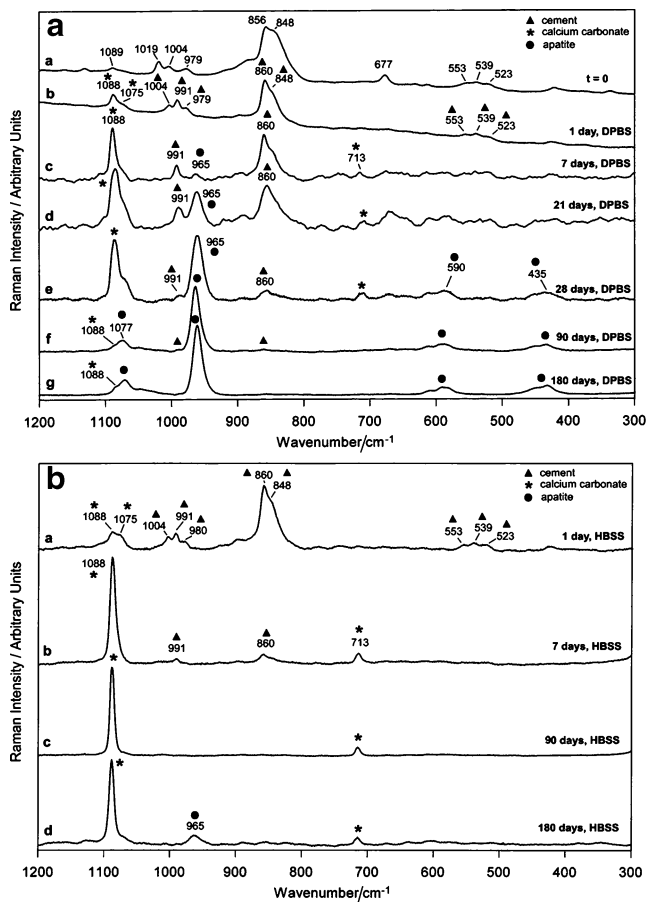


**Fig. 4** Raman spectra showing the chemical transformations of the upper surface of the wTC cement during ageing in DPBS (a) and HBSS (b)

(apatite) deposits on the cement surface. The data indicated that apatite deposits are already present on 14-day DPBS-aged samples. After 28 days, SEM-EDX on the samples stored in DPBS showed a homogeneous Ca- and P-rich coating layer primarily constituted by calcium-phosphate (apatite) and calcium-carbonate (calcite) deposits and by carbonated apatite and calcite after 90–180 days, as demonstrated by micro-Raman. The thickness of the apatite–calcite coating layer increased over soaking time

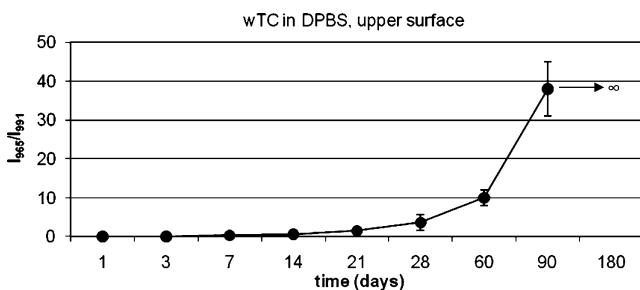


**Fig. 5** Trend of the Raman  $I_{965}/I_{991}$  intensity ratio (average of five measurements  $\pm$  standard deviation) calculated from the spectra recorded on the outer surface of wTC during ageing in DPBS

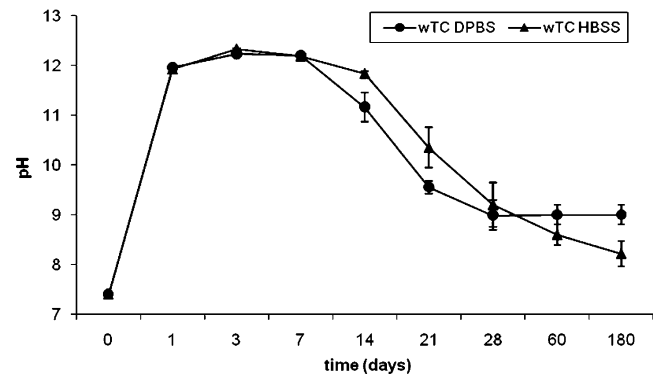


**Fig. 6** pH (average of three measurements  $\pm$  standard deviation) of the two soaking solutions at different times

attaining approximately 900  $\mu\text{m}$  after 180 days of ageing in DPBS.

The bioactivity of Portland cement in highly concentrated phosphate-buffered solutions has been recently reported both in medium-term [32] and short-term studies [12, 26, 32]. This is the first investigation on the bioactivity of calcium-silicate cement after long soaking times in both high- and low-phosphate-containing solutions, and the first which analyses the biological activity of this cement using Raman spectroscopy.

Coleman et al. [11, 32] investigated the in vitro apatite layer formation in a ground Portland cement-SBF system, whereas Tay et al. [12] showed the formation of calcium-deficient apatite precipitates in a Portland cement-PBS system. Gallego et al. [26] observed apatite-like and calcite crystals on set Portland cement exposed to phosphate solution and  $\text{CO}_2$  and apatite-like phase formation on carbonated substrates. Calcium ions supplied by the hydration-derived basic calcium hydroxide (portlandite) can react with the environmental carbonate ions forming calcium carbonate (calcite). The crystalline form of calcium carbonate as calcite formed on cement surface by carbonation process showed good biological activity [33, 34] and positively affected the cytocompatibility [26]. Soluble portlandite crystals allow the nucleation of calcium carbonate polymorphs and/or metastable calcium salt crystals that readily transform into the stable calcite phase in water [33]. Calcium carbonate may precipitate at the surface and in the cement paste porosity forming a protective layer of calcium carbonate on the outer zone of cement discs [35]. The protective calcium carbonate layer constrains or reduces the ionic diffusion from cement bulk and probably decreases its degradation and may improve the marginal sealing of root-end filling restorations [9, 36].

The cement used in the present study revealed the formation of a superficial Ca-rich layer (calcium carbonate or calcite layer) on the surface after soaking in both physiological-like phosphate solutions. Micro-Raman spec-



troscopy confirmed the presence on the cement surface of carbonate ions in different chemical phases, mainly as calcite. Calcium ions supplied by the rapid dissolution of portlandite and by the cement matrix can react with environmental carbonate ions to form a calcium carbonate superficial layer [35]. This Ca-rich layer may absorb phosphate from the soaking solution allowing the crystallisation of apatite crystals, as confirmed by micro-Raman analysis. The apatite content in the coating layer increased over soaking time. The high pH of both soaking media detected at all the investigated ageing times reflects the progressive hydration of silicate species and the rapid and continuous dissolution of calcium hydroxide from the cement matrix. Moreover, the Raman analysis of the fractured samples aged in DPBS for 180 days detected carbonated apatite until 900  $\mu\text{m}$  from the cement disc surface demonstrating the high thickness of the carbonated apatite coating layer.

The cement bioactivity in HBSS was less noticeable than in DPBS, according to the lower phosphate concentration of HBSS. HBSS was selected to have a commercially available standardised soaking medium mimicking the composition of inorganic ions of human blood plasma, without representing a supersaturated solution with respect to apatite. HBSS contains lower calcium and same phosphate concentration than human plasma and was already used in bioactivity studies and in tissue engineering or culture cell culture studies [37, 38]. The higher amounts of calcite detected on the surface of cement soaked in HBSS is related to the presence of carbonate ions in this medium. The surface showed small Ca-rich crystals after 1–14 days. Sparse cloud-like Ca- and P-containing deposits appeared after 14 days in agreement with the 965- $\text{cm}^{-1}$  phosphate band detected in the Raman spectrum of the powder isolated from the storage medium. After 180 days of ageing in HBSS, the deposit thickened (so that the 965- $\text{cm}^{-1}$  band also became detectable on the surface) and the entire surface appeared covered by a light porous matrix of carbonated apatite with interspersed polygonal crystals of calcite forming a porous and inhomogeneous apatite–calcite coating layer less than 50  $\mu\text{m}$  thick.

This study demonstrated the *in vitro* bioactivity of the experimental calcium-silicate cement and supports the hypothesis that the apatite biocoating formed on Portland cements and MTAs may play a clinical positive role by promoting the adsorption of proteins, the osteoblast adhesion and proliferation [39–46] and bone bonding and healing when used *in vivo* as root-end filling material [47, 48]. The clinical implementation of calcium-silicate portland cements may exploit the bioactivity properties of bone-like apatite-forming materials [41] for bone production [47, 48] and dentin bridge formation [49, 50].

## Conclusions

Calcium hydroxide (portlandite) was rapidly depleted from the calcium-silicate cement matrix subsequently forming a thick layer of calcium-carbonate (calcite) and calcium-phosphate (apatite). SEM-EDX and micro-Raman analyses showed the ability of these cements to produce a bone-like apatite coating. The contact and the interaction of the calcium-silicate hydraulic cement with different physiological environments affect its surface morphology and surface chemical composition.

**Conflict of Interest** The authors declare that they have no conflict of interest.

## References

1. Camilleri J, Montesin FE, Brady K, Sweeney R, Curtis R, Pitt Ford TR (2005) The constitution of mineral trioxide aggregate. *Dent Mater* 21:297–303
2. Saunders WP (2008) A prospective clinical study of periradicular surgery using mineral trioxide aggregate as a root-end filling. *J Endod* 34:660–665
3. Pace R, Giuliani V, Pagavino G (2008) Mineral trioxide aggregate as repair material for furcal perforation: case series. *J Endod* 34:1130–1133
4. Holden DT, Schwartz SA, Kirkpatrick TC, Schindler WG (2008) Clinical outcomes of artificial root-end barriers with mineral trioxide aggregate in teeth with immature apices. *J Endod* 34:812–817
5. Gandolfi MG, Farascioni S, Pashley DH, Gasparotto G, Prati C (2008) Calcium silicate coating derived from Portland cement as treatment for hypersensitive dentine. *J Dent* 36:565–578
6. Nair PNR, Duncan HF, Pitt-Ford TR, Luder HU (2009) Histological, ultrastructural and quantitative investigations on the response of healthy human pulps to experimental capping with mineral trioxide aggregate: a randomized controlled trial. *Int Endod J* 42:422–444
7. Torabinejad M, White DJ (1995) US Patent Number, 5,769,638
8. Camilleri J (2007) Hydration mechanisms of mineral trioxide aggregate. *Int Endod J* 40:462–470
9. Sarkar NK, Caicedo R, Ritwik P, Moiseyeva R, Kawashima I (2005) Physicochemical basis of the biologic properties of mineral trioxide aggregate. *J Endod* 31:97–100
10. Bozeman TB, Lemon RR, Eleazer PD (2006) Elemental analysis of zirconal precipitates from gray and white MTA. *J Endod* 32:425–428
11. Coleman NJ, Nicholson JW, Awosanya K (2007) A preliminary investigation of the *in vitro* bioactivity of white Portland cement. *Cem Concr Res* 37:1518–1523
12. Tay FR, Pashley DH, Rueggeberg FA, Loushine RJ, Weller RN (2007) Calcium-phosphate phase transformation produced by the interaction of the Portland cement component of white mineral trioxide aggregate with a phosphate-containing fluid. *J Endod* 33:1347–1351
13. Tay FR, Pashley DH (2008) Guided tissue remineralisation of partially demineralised human dentine. *Biomaterials* 29:1127–1137
14. Ding SJ, Kao CT, Shie MY, CJr H, Huang TH (2008) The physical and cytological properties of white MTA mixed with  $\text{Na}_2\text{HPO}_4$  as an accelerant. *J Endod* 34:748–751

15. Chng HK, Islam I, Yap AUJ, Tong YW, Koh ET (2005) Properties of a new root-end filling material. *J Endod* 31:665–668
16. Islam I, Chng HK, Adrian U, Yap UJ (2006) Comparison of the physical and mechanical properties of MTA and Portland cement. *J Endod* 32:193–197
17. Wiltblank KB, Schwartz SA, Schindler WG (2007) Effect of selected accelerants on the physical properties of Mineral Trioxide Aggregate and Portland cement. *J Endod* 33:1235–1238
18. Abdullah D, Ford TR, Papaioannou S, Nicholson J, McDonald F (2002) An evaluation of accelerated Portland cement as a restorative material. *Biomaterials* 23:4001–4010
19. Kogan P, He J, Glickman GN, Watanabe I (2006) The effects of various additives on setting properties of WMTA. *J Endod* 32:569–572
20. Nelson DGA, Featherstone JDB (1982) Preparation, analysis and characterization of carbonated apatites. *Calcif Tissue Int* 34:S69–S75
21. Black L, Breen C, Yarwood J, Deng CS, Phipps J, Maitland G (2006) Hydration of tricalcium aluminate (C3A) in the presence and absence of gypsum – studied by Raman spectroscopy and X-ray diffraction. *J Mater Chem* 16:1263–1272
22. Sarma LP, Prasad PSR, Ravikumar N (1998) Raman spectroscopic study of phase transitions in natural gypsum. *J Raman Spectrosc* 29:851–856
23. Tarrida M, Madon M, Le Rolland B, Colombet P (1995) An in-situ Raman spectroscopy study of the hydration of tricalcium silicate. *Adv Cem Based Mater* 2:15–20
24. Gastaldi D, Boccaleri E, Canonico F, Bianchi M (2007) The use of Raman spectroscopy as a versatile characterization tool for calcium sulphoaluminate cements: a compositional and hydration study. *J Mater Sci* 42:8426–8432
25. Martinez-Ramirez S, Frias M, Domingo C (2006) Micro-Raman spectroscopy in white Portland cement hydration: long-term study at room temperature. *J Raman Spectrosc* 37:555–561
26. Gallego D, Higueta N, Garcia F, Ferrel N, Hansford DJ (2008) Bioactive coatings on Portland cement substrates: Surface precipitation of apatite-like crystals. *Mater Sci Engin* 28:347–352
27. Potgieter-Vermaak SS, Potgieter JH, Van Grieken R (2006) The application of Raman spectrometry to investigate and characterize cement, part I: a review. *Cem Concr Res* 36:656–662
28. Taddei P, Tinti A, Gandolfi MG, Rossi PL, Prati C (2009) Vibrational study on the bioactivity of portland cement-based materials for endodontic use. *J Mol Structure* 924–926:548–554
29. Takita T, Hayashi M, Takeiti O, Ogiso B, Suzuki N, Otsuka K, Ito K (2006) Effect of mineral trioxide aggregate on proliferation of cultured human dental pulp cells. *Int Endod J* 39:415–422
30. Tuna D, Ölmez A (2008) Clinical long-term evaluation of MTA as a direct pulp capping material in primary teeth. *Int Endod J* 41:273–278
31. Siqueira JF, Guimaraes-Pinto T, Rôças IN (2007) Effect of chemomechanical preparation with 2.5% sodium hypochlorite and intracanal medication with calcium hydroxide on cultivable bacteria in infected root canals. *J Endod* 33:800–805
32. Coleman NJ, Awosanya K, Nicholson JW (2009) Aspects of the in vitro bioactivity of hydraulic calcium (aluminosilicate) cement. *J Biomed Mater Res Part 90A*:166–174
33. Zhao W, Wang J, Zhai W, Wang Z, Chang J (2005) The self-setting properties and in vitro bioactivity of tricalcium silicate. *Biomaterials* 26:6113–6121
34. Fujita Y, Yamamuro T, Nakamura T, Kotani S, Ohtsuki C, Kokubo T (1991) The bonding behavior of calcite to bone. *J Biomed Mater Res* 25:991–1003
35. Kamali S, Moranville M, Leclercq S (2008) Material and environmental parameter effects on the leaching of cement pastes: experiments and modelling. *Cem Concr Res* 38:575–585
36. Gandolfi MG, Sauro S, Mannocci F, Zanna S, Capoferri M, Prati C, Mongiorgi R (2007) New tetrasilicate cement as retrograde filling material: an in vitro study on fluid penetration. *J Endod* 33:1082–1085
37. Shie MY, Chen DCH, Wang CY, Chiang TY, Ding SJ (2008) Immersion behaviour of gelatine-containing calcium phosphate cement. *Acta Biomater* 4:646–655
38. Kokubo T, Takadama H (2006) How useful is SBF in predicting in vivo bone bioactivity? *Biomaterials* 27:2907–2915
39. Gandolfi MG, Perut F, Ciapetti G, Mongiorgi R, Prati C (2008) New Portland cement-based materials for endodontics mixed with articaine solution: a study of cellular response. *J Endod* 34:39–44
40. Gandolfi MG, Pagani S, Perut F, Ciapetti G, Baldini N, Mongiorgi R, Prati C (2008) Innovative silicate-based cements for endodontics: a study of osteoblast-like cell response. *J Biomed Mater Res* 86(A):477–486
41. Gandolfi MG, Ciapetti G, Perut F, Taddei P, Modena E, Rossi PL, Prati C (2009) Biomimetic calcium-silicate cements aged in simulated body solutions. Osteoblasts response and analyses of apatite coating. *J Appl Biomater Biomech*, in press
42. Camilleri J, Montesin FE, Di Silvio L, Pitt Ford TR (2005) The chemical constitution and biocompatibility of accelerated Portland cement for endodontic use. *Int Endod J* 38:834–842
43. Ribeiro DA, Duarte MA, Matsumoto MA, Marques ME, Salvadori DM (2005) Biocompatibility in vitro tests of mineral trioxide aggregate and regular and white Portland cements. *J Endod* 31:605–607
44. Koh ET, Torabinejad M, Pitt Ford TR, Brady K, McDonald F (1997) Mineral trioxide aggregate stimulates a biological response in human osteoblasts. *J Biomed Mater Res* 37:432–439
45. Al-Rabeah E, Perinpanayagam H, MacFarland D (2006) Human alveolar bone cells interact with ProRoot and tooth-colored MTA. *J Endod* 32:872–875
46. Chen CL, Huang TH, Ding SJ et al (2009) Comparison of calcium silicate cement and mineral trioxide aggregate biologic effects and bone markers expression in MG63 cells. *J Endod* 35:682–685
47. Saidon J, He J, Zhu Q, Safavi K, Spångberg LS (2003) Cell and tissue reactions to mineral trioxide aggregate and Portland cement. *Oral Surg Oral Med Oral Pathol Oral Radiol Endod* 95:483–489
48. Torabinejad M, Pitt Ford TR, McKendry DJ, Kariyawan SP et al (2009) Histologic assessment of mineral trioxide aggregate as root-end filling in monkeys. *Int Endod J* 42:408–411
49. Masuda-Murakami Y, Kobayashi M, Wang X, Yamada Y, Kimura Y, Hossain M, Matsumoto K (2009) Effects of mineral trioxide aggregate on the differentiation of rat dental pulp cells. *Acta Histochem*, doi:10.1016/j.acthis.2009.05.001
50. Min KS, Park HJ, Lee SK, Park SH, Hong CU, Kim HW, Lee HH, Kim EC (2008) Effect of mineral trioxide aggregate on dentin bridge formation and expression of dentin sialoprotein and heme oxygenase-1 in human dental pulp. *J Endod* 34:666–670